HHS Public Access

Author manuscript

Magn Reson Med. Author manuscript; available in PMC 2019 May 01.

Published in final edited form as:

Magn Reson Med. 2019 May ; 81(5): 3406–3415. doi:10.1002/mrm.27637.

Size-adaptable "Trellis" structure for tailored MRI coil arrays

Bei Zhang[1,2], **Ryan Brown**[1,2,3], **Martijn Cloos**[1,2,3,4], **Riccardo Lattanzi**[1,2,3], **Daniel Sodickson**[1,2,3,4], and **Graham Wiggins**[*]

[1]Bernard and Irene Schwartz Center for Biomedical Imaging, New York University School of Medicine, New York, New York

[2]Center for Advanced Imaging Innovation and Research, New York University School of Medicine, New York, New York

[3]Sackler Institute of Graduate Biomedical Sciences, New York University School of Medicine, New York, New York

[4]Tech4Health, NYU Langone Health, New York

Abstract

Purpose: We present a novel, geometrically adjustable, receive coil array whose diameter can be tailored to the subject in order to maximize sensitivity for a range of body sizes.

Theory and Methods: A key mechanical feature of the size-adaptable receive array is its trellis structure that was motivated by similar structures found in gardening and fencing. Our implementation is a cylindrical trellis that features encircling, diagonally interleaved slats, which are linked together at intersecting points. The ensemble allows expansion or contraction to be controlled with the angle between the slats. This mechanical frame provides a base for radiofrequency coils wherein approximately constant overlap, and therefore coupling between adjacent elements, is maintained when the trellis is expanded or contracted. We demonstrate 2 trellis coil concepts for imaging lower extremity at 3T: a single-row 8-channel array built on a trellis support structure and a multirow 24-channel array in which the coil elements themselves form the trellis structure.

Results: We show that the adjustable trellis array can accommodate a range of subject sizes with robust signal-to-noise ratio, loading, and coupling.

Conclusion: The trellis coil concept enables an array of surface coils to expand and contract with negligible effect on tuning, matching, and decoupling. This allows an encircling array to conform closely to anatomy of various sizes, which provides significant gains in signal-to-noise ratio.

Keywords

coupling; phased-array; preamplifier noise; stretchable; trellis

Correspondence Bei Zhang, NYU Langone Radiology— Center for Biomedical Imaging, 660 1st Avenue, New York, NY 10016-6402, USA., bei.zhang@nyulangone.org.

[*]Deceased

1 | INTRODUCTION

Multiple-receive-element arrays[1] are widely used in MRI because of their high sensitivity and parallel imaging capability.[2–4] Intuitively, one expects that the array should fit tightly to the subject in order to maximize signal sensitivity over a large region of interest.[5–9] However, it is not possible to obtain the same filling factor for diverse subject sizes with rigid coils, which is typically the case in practical settings. Rigid coils are usually made large enough to also accommodate relatively large-size subjects, thus sacrificing potential signal- to-noise ratio (SNR) in small-size subjects.

Commercially available flexible planar arrays can conform, to some degree, to a range of body sizes, but are not optimal for encircling anatomies, such as extremities or torso because of undesirable element overlaps or gaps in coverage. The research community has further advanced flexible coil technology by demonstrating a variety of techniques. Nordmeyer-Massner et al replaced conventional semirigid circuit board substrate with woven copper conductors mounted on stretchable fabric to image the knee over a range of flexion angles[10,11]; Corea et al helped open the door for wearable coils by printing conductive ink onto thin, flexible plastic film[12]; X. Yan et al proposed an imbalanced capacitor distribution such that magnetic and electric coupling cancel each other to form a self-decoupled loop, which can provide robust SNR that is independent of coil spacing within an array[13,14]; and some others have demonstrated a range of novel electromechanical structures and materials.[15–18] Whereas these developments generally focused on substrate flexibility and/or reducing coupling, we saw an opportunity to create a new coil structure that provides encircling coverage of cylindrical objects over a range of diameters without coverage overlap or gaps. The main challenges in building such an adjustable array are to design a flexible substrate that minimizes the distance between the coil and object while simultaneously minimizing shifts in tuning and matching that arise from positioning changes, which can reduce SNR, attributed to nonoptimal noise matching[19] and coil coupling, which injects preamplifier noise into the multiple-channel receive coil.[9,20]

In this work, we introduce the “trellis” structure for size-adaptable coil array designs. We designed and built 2 arrays by judiciously mounting coil elements to a trellis framework and arranging the coil elements themselves into a trellis structure respectively. One is an 8-channel, 1-row array attached to a Teflon trellis structure in which each coil element has a rectangular shape; the other is a 24-channel, 3-row array arranged into a trellis structure by linking conductors. We demonstrated performance of both coil arrays in various-size phantoms, and in vivo capability of the 24-channel trellis array was subsequently demonstrated in the lower extremities.

2 | METHODS

2.1 | 8-channel array

We built an 8-channel array on a trellis structure, formed by a 2-layer criss-crossed network of 72 nylon slats (5 mm wide × 342 mm long × 2.4 mm thick), cut out with a routing machine (Quick Circuit 7000; T-Tech, Inc., Peachtree Corners, GA) from $3/32'' \times 12'' \times 24''$ nylon sheets (8539K32; McMaster-Carr, Robbinsville, NJ) that were linked by 3D

printed polycarbonate clamps consisting of a half-spherical ferrule flange and a cap (CAD files can be provided per request) every 5.7 mm (Figure 1). The structure had a diameter that can be expanded from 145 to 205 mm by adjusting the angle between the slats.

Each coil element was made of 4 independent rigid copper slats that were joined with flexible jumper wires. The rigid copper slats were routed from 0.031-mil-thick single-sided circuit board (T-Tech, Inc.). The slats were 6 mm in width and 54 mm in length with two 6.4-mm-long slots located at each third of the length. Two gaps were included between the slots for a tuning capacitor and jumping wire (8050, BELDEN 20AWG copper wire; Belden Inc., St. Louis, MO). Flexible multistrand wire (0.4 mm in diameter; ODU-USA, Inc., Camarillo, CA) was routed around screw locators at the corners of each coil to link the circuit boards and define the coil shape.

By using 10 nylon strips per coil element width, the critical 10% coil overlap can be maintained,[1] as indicated in Figure 1. When the coil width is w_1, the overlap is $0.1 \times w_1$, and when the trellis substrate is squeezed and the coil width is reduced to w_2, the overlap is correspondingly changed to $0.1 \times w_2$, which means that the 10% overlap is maintained. The lattice can expand in diameter from 145 to 205 mm, morphing each coil element from 65 × 95 mm to 95 × 65 mm in the process (Figure 3). Each element was tuned to 123.2 MHz, the operating frequency of our 3T MR scanners, whereas the array was configured with a nominal diameter of 165 mm and loaded with a water phantom of the same diameter to approximate the 99% percentile male knee.[21] To determine coil variability in a range of subject sizes, we measured the scattering matrix in the above phantom and 2 others (134 and 195 mm in diameter, representing 50th and 99th percentile knee size, respectively). All phantoms were filled with salt and sucrose to approximate dielectric properties of the human knee at 3T (38.7 g of salt and 1341.5 g of sucrose per 1 L of water to generate $\varepsilon_r = 56.6$ and $\sigma = 0.37$ S/m).[22,23]

The individual coils had an active detuning circuit formed by the 68-pF matching capacitor at the port, which is in parallel with a hand-wound inductor and a positive-intrinsic-negative (PIN) diode (MA4P4002B-402; Macom, Lowell, MA). The schematic drawing of each coil element is shown in Figure 1B. When a 100-mA DC current flows through the PIN diode, the 68-pF matching capacitor and the hand-wound inductor form an open circuit at the port, thus detuning the coil during body coil transmission. The coils were connected to an 8-channel preamplifier fixture holding 8 preamplifiers (Siemens, Erlangen, Germany) with 387-mm-long RG316 coaxial cables (Coast Wire & Plastic Tech LLC, Carson, CA) whose lengths were adjusted to achieve preamplifier decoupling.

The SNR provided by the 8-channel trellis array and was compared with the SNR of a commercially available 15-channel knee coil (154-mm inner diameter and 256-mm length; Quality Electrodynamics [QED], Mayville, OH)[24] for the 3 phantoms described above (see Table 1 for scan parameters). Measurements were performed on a whole-body 3T system (Prisma or Biograph mMR; Siemens).

2.2 | 24-channel array

The second array we built was a 3-row, 24-channel trellis coil (Figure 2), which consisted of a combination of 3 different slat elements that were connected to create diamond-shaped coils with 75-mm length. The slabs were made of 1-sided 0.031-mil printed circuit board (PCB) board and 3 different circuit board pieces (Figure 2). The side of each diamond was 75 mm in length and 3 mm in width. This configuration allowed coil decoupling between various neighbors: Intrarow decoupling was provided by geometric overlap at the coil corners, adjacent-row decoupling by overlapped edges, and the first and third rows by shared capacitors. Rivets, whose position was determined by the required overlap for decoupling, linked the pivot points, with the slats linked together by short, flexible jumping wires. We used approximately 18-mm-long wire that allowed intersecting slats to vary between 70 and 120 mm, which resulted in a diameter range from 125 to 215 mm. These dimensions correspond to 50th to 99th percentile of human knee sizes.[21] Each coil element was tuned to 123.2 MHz while loaded with the 195-mm-diameter phantom. The schematic drawing of each coil element is shown in Figure 2. In order to place the preamplifier (DaVinci; Siemens) directly at the port, the matching circuit consists of a 27-pF capacitor at the port and 22-pF capacitor in series with the signal line to achieve preamplifier decoupling (Figure 2C). To disable the array during body coil transmission, an active detuning circuit formed by a 27-pF tuning capacitor next to the port, a hand-wound inductor and a PIN diode was installed on each coil. The active detuning circuit and the radiofrequency (RF) signal shared the ground connection (Figure 2C). Active detuning current suppression was measured for an unloaded coil element because the change in S12 with a double pick-up probe with and without bias applied to the PIN diode. Similarly, the achieved degree of preamplifier decoupling was measured for an unloaded coil element because the change in S12 detected by the double pick-up probe when the coil was matched to a 50-ohm load, or when the preamplifier was powered to achieve the decoupling condition. Isolation between a pair of coil elements was determined from an S12 measurement with the pair of coil elements matched to 50 ohms and directly coupled to 2 ports of a network analyzer while all other coil elements were detuned. The unloaded-to-loaded Q ratio of the designed trellis coil element was estimated from the S12 measurement of a single coil element in the middle row of the array, using the double pick-up probe, loosely coupled to the coil element, while all other coil elements were detuned.

The SNR of the 24-ch (channel) array was compared to the 15-channel QED knee coil (see previous section) for the 134-mm phantom. Because the 195-mm phantom cannot be accommodated in the QED coil, for this validation, we used the Siemens Body 18[25] (overall dimensions: 385 × 590 × 65 mm).

2.3 | In-vivo experiments

In-vivo imaging and SNR measurements were performed upon approval by our local Institutional Review Board and with informed written consent from 1 volunteer. We scanned the volunteer's knee using both the 24-ch trellis array and the 15-channel QED knee coil on the Biograph mMR. To simulate the knee of a large subject, we scanned the thigh of the same volunteer using both the expanded 24-ch trellis array and the combination of the system flex array[26] (wrapped around the top part of the thigh) with the system spine array

(on the bottom of the patient bed), which is the routine setup at our institution for large subjects. Scanning parameters for the knee and thigh imaging are listed in Table 1.

2.4 | SNR and g-factor measurements

Gradient echo data (see Table 1 for imaging parameters) were obtained in the sagittal, transverse, and coronal planes. A noise reference measurement was also obtained by recording complex-valued raw data with the same pulse sequence used for the image acquisition, but with no RF excitation. Data analysis was performed offline with custom software written in Matlab (The MathWorks, Inc., Natick, MA). The noise covariance matrix was calculated from the statistics of the noise samples scaled by dividing the sample covariance matrix by the scalar-valued noise equivalent bandwidth to account for noise autocorrelations within each channel attributed to the filtering introduced by the data acquisition electronics and receiver.[27] Receive sensitivity profiles estimates were obtained by dividing individual coil images by the square root of the sum of squares combination of all coils, which is a good approximation for encircling arrays. With coil sensitivity estimates and channel noise covariance estimates in hand, composite images in absolute SNR units were obtained following the general procedure outlined by Kellman and McVeigh.[27] The noise coefficient matrix was computed from the noise covariance matrix in each case, and the mean and maximum values of its off-diagonal elements were recorded. Maps of the g factor distribution were calculated to simulate coil performance for various acceleration factors.

3 | RESULTS

3.1 | 8-channel array

The 8-channel trellis array diameter varied from 145 to 205 mm, which can accommodate 1st ~ 99th percentile of knee sizes.[21] The unloaded-to-loaded Q ratio of an individual coil was 6.57 (230/35) and 4.6 (230/50) when loaded with the 195- and the 134-mm phantom, respectively. This compares to a Q ratio of 10.5 (337/32) for a conventional rigid coil element of the same size placed 3 mm (the thickness of the trellis frame) away from the large phantom. The elements of the 8-channel array were tuned and matched to 50 ohm using the 165-mm-diameter phantom, and decoupling was adjusted by moving a wire jumper on the circuit board. Once this was set, no additional adjustments were made to the array as it was expanded and contracted on the different sized phantoms. S-parameter plots for a pair of coils are shown at the bottom of Figure 4. With the trellis structure wrapped tightly around each of the 3 phantoms, coil tuning changed by <1.2 MHz, whereas matching and decoupling were <–12.0 and –10.7 dB, respectively.

With the trellis size adjusted to minimize the distance between the coil and phantoms, the SNR at the center was 546.2, 391.2, and 286.9 for the 134-, 165-, and 195-mm phantoms, respectively. For comparison, the SNR provided by the commercial coil (fixed diameter of 160 mm) was 464.4 at the center of the 134-mm-diameter phantom, which is 15% lower than for the trellis. Note that the other phantoms were too large to fit into the commercial coil. The SNR was 435.5 in the center of the 134-mm phantom when the trellis diameter was

195 mm (Figure 4, fourth column). Mean and maximum values of the off-diagonal elements in each case were provided at the bottom of Figure 4.

3.2 | 24-channel array

The 24-channel trellis array was tuned on the 195-mm phantom, with match and coupling levels smaller than –16 and –9.1 dB, respectively (Figure 5). The Q ratio was 7.13 (214/30). Preamplifier decoupling was <–15 dB and active detuning <–25 dB for all coils. Without retuning the coil, the match and coupling levels were smaller than –10.5 and –11 dB, respectively, when the trellis was wrapped onto the 165-mm phantom. They were <–4.7 and <–7.5 dB for the 134-mm phantom.

The 24-channel array resulted in a 40% SNR gain in the center of the 134-mm phantom compared to the commercial coil (Figure 6), with both coils providing similar longitudinal coverage.

The 24-channel trellis array provided similar SNR (within 1%) at the center of the 195-mm phantom and up to 1.73-fold SNR increase in the periphery, compared to the Siemens body 18 (which is used to image large subjects at our clinical center).

Figure 7 compares the g-factor for the 24-channel trellis coil, the QED 15-channel knee coil, and the 18-channel Siemens flexible body array for 1D acceleration in the right-left (RL) direction and for 2D acceleration in the RL and anterior-posterior (AP) directions. The 24-channel trellis array shows excellent parallel imaging performance in both the AP and LR directions. Acceleration by a factor of 2 × 2 entailed very little noise amplification. Acceleration by a factor of 4 in the AP direction resulted in moderate, but still acceptable, noise amplification. The maximum g-factor value was reported at the bottom of each map.

In vivo measurements in the knee (diameter approximately 130 mm) show that the SNR for the 24-channel trellis array was approximately 51% higher in the center and 117% higher in the periphery than the commercial knee array (Figure 8), while also yielding a broader sensitivity coverage. Similarly, SNR maps in the thigh of the same subject (diameter approximately 160 mm; Figure 9) showed a 50% SNR gain for the trellis array over the combination of the flexible body array with the spine array (the standard clinical setup at our center), demonstrating the adaptability of the trellis array to different anatomies.

4 | DISCUSSION

The trellis structure enabled size-adaptable coil arrays that minimized the distance between the coil and sample. The geometric layout naturally maintained adequate tuning and decoupling between neighbor coils while its size was adapted to various sample sizes.

By minimizing both distance to the sample and tuning variability, the trellis arrays outperformed dedicated commercial coils in phantom and in vivo experiments.

The main advantage of the trellis design is that 1 array can be close to optimal performance for various patient sizes. We demonstrated a >50% SNR boost in both the knee and thigh with the same 24-channel trellis array compared to its clinical peers. Moreover, our results

demonstrated that we can use just 1 trellis coil for different applications, because it is adaptable.

When we change the diameter of the trellis structure, the perimeter of each coil element does not change, but its area does. In fact, the area of each coil element is largest when the coil is square and smallest when the array is expanded to the largest diameter or squeezed to the smallest diameter. This change in the coil's area can affect both tuning and matching. In this work, the tuning and matching change attributed to variations in coil element area were not significant for the 8-channel trellis array, because the change of wire length on 1 side (e.g., the width) was compensated by the opposite change on its perpendicular side. As a result, the ratio of minimal-to-maximal area on different phantoms was 0.96, resulting in tolerable S-parameter changes (Figure 3). For the 24-channel trellis array, the angle of the diamond changed from 97.8° on the large phantom to 62.4° on the small phantom, resulting in a ratio of 0.89 between the minimal and maximal areas, which gave rise to more significant S-parameter changes on different phantoms. We chose to optimize the S parameters on the large phantom rather than on the smallest phantom. Working in our favor is that the coil fitted closely to all phantoms, thus providing SNR benefits that outweighed impedance mismatching (Figure 6).

We tuned and decoupled the trellis coil elements in the presence of the 195-mm phantom, which was the largest in our study. The ratio of central SNR for the smallest phantom to the largest phantom was 1.9 for the 8-channel trellis array and 2.1 for the 24-channel trellis array. This suggests that the high reflection coefficients of the 24-channel trellis array in the case of the small phantom do not have a significant effect on the SNR when the coil is heavily loaded. From Figure 4, we can see that the z-extent of the 8-channel trellis array shrinks as the array diameter increases. The central SNR for the large phantom has been improved after adding extra rows. Increasing the z-extent of the array also enabled a fairer comparison with the QED coil, which has a larger coverage in the z direction. We also confirmed the benefits of having the coil conform closely to the phantom, because we clearly showed SNR degradation when we compared to data obtained with the trellis coil at maximum diameter, but with the smallest phantom as the sample. In particular, when the coil expanded to the size of largest phantom, the SNR dropped by nearly 30%, demonstrating the importance of a close-fitting geometry to obtain the optimal SNR (Figures 4 and 6, third versus fourth columns).

One feature of the single-row 8-channel trellis array is the robust tuning owing to the approximately fixed coil perimeter with respect to the overall diameter (Figure 3, bottom). The geometry also provided good decoupling between adjacent (square) coils by maintaining roughly 10% overlap. However, this decoupling configuration was not extendable to multiple rows because of the inverse correlation between trellis diameter and inter-row overlap. In order to overcome this limitation, we implemented diamond-shaped coils whose overlapped vertices, and therefore coil coupling, were less sensitive to changes in trellis diameter. In practice, we found that the 24-channel multirow array provided similar coverage, but improved performance compared to a state-of-the-art clinical knee coil.

In this work, we applied the trellis coil to lower extremities imaging because of the wide variability of this anatomical region. One could readily extend the trellis concept to other applications, such as the upper extremities, torso, or pediatrics imaging. Furthermore, we focused exclusively on receive-only coils, whose SNR is desensitized to the effect of coil coupling by the use of preamplifier decoupling. In a previous study, we applied the trellis concept to improve transmit efficiency by minimizing the distance between the object and coil in a sparse transmit/receive array,[28] in which intercoil coupling was not substantial. To apply the trellis design to dense transmit arrays, additional care will be required to mitigate coupling.

The arrays constructed for this work included makeshift housing shells that were sufficient to demonstrate the trellis concept. In order to translate the concept to routine clinical practice, one would need to develop a durable shell that does not restrict mechanical flexibility. The housing should allow the coils, preamplifiers, and cabling to move smoothly over a range of positions. One could imagine an overlapping patchwork of telescoped protective layers to satisfy these requirements. Although these are certainly key considerations for practical implementation, we believe that they are beyond the scope of this work, in which we focus on prototype performance evaluation.

In recent years, a wide variety of ultraflexible and wearable MRI coils have been introduced in the literature,[12,29–31] which use elegant means to achieve mechanical flexibility and coil decoupling, such as current limiting preamplifiers, clever matching interfaces, and printed or woven conductors. We believe that the fundamental electromagnetic detector circuitry and thus the underlying SNR and Q to be similar in each example; their unique set of advantageous mechanical features must be considered with respect to the desired application. For example, although the trellis concept provides gains over rigid coils in cylindrically shaped samples, it may not be well suited for dynamic studies of joint motion.[30,31]

5 | CONCLUSION

The use of a trellis coil concept enables an array of surface coils to expand and contract with only minor shifts in tune, match, and decoupling. This allows an encircling array to conform closely to anatomy of various sizes, which provides significant SNR gains over conventional coils that are usually designed as 1 size fits all. We applied the trellis concept to design a receive array consisting of loops of various geometries for lower-extremity MRI. The same idea can be extended to other anatomical regions, such as upper extremities and torso, to pediatric imaging as well as other topologies, including transmit/receive and electric dipole arrays.

ACKNOWLEDGMENT

This work is dedicated to Dr Graham Wiggins (1962–2016), who left us 2 years ago but blesses us from afar. The trellis coil design was invented by Dr Graham Wiggins (United States Patent Application No. 20180045794). Dr Bei Zhang built the coils under Graham's guidance.

Funding information

This work was performed under the rubric of the Center for Advanced Imaging Innovation and Research (www.cai2r.net), a NIBIB Biomedical Technology Resource Center (NIH P41 EB017183).

REFERENCES

1. Roemer PB, Edelstein WA, Hayes CE, Souza SP, Mueller OM. The NMR phased array. Magn Reson Med 1990;16:192–225. [PubMed: 2266841]
2. Sodickson DK, Manning WJ. Simultaneous acquisition of spatial harmonics (SMASH): fast imaging with radiofrequency coil arrays. Magn Reson Med 1997;38:591–603. [PubMed: 9324327]
3. Pruessmann KP, Weiger M, Scheidegger MB, Boesiger P. SENSE: sensitivity encoding for fast MRI. Magn Reson Med 1999;42:952–962. [PubMed: 10542355]
4. Griswold MA, Jakob PM, Heidemann RM, et al. Generalized autocalibrating partially parallel acquisitions (GRAPPA). Magn Reson Med 2002;47:1202–1210. [PubMed: 12111967]
5. Lattanzi R, Grant AK, Polimeni JR, et al. Performance evaluation of a 32-element head array with respect to the ultimate intrinsic SNR. NMR Biomed 2010;23:142–151. [PubMed: 19904727]
6. Wiggins GC, Polimeni JR, Potthast A, Schmitt M, Alagappan V, Wald LL. 96-Channel receive-only head coil for 3 Tesla: design optimization and evaluation. Magn Reson Med 2009;62:754–762. [PubMed: 19623621]
7. Wiggins GC, Triantafyllou C, Potthast A, Reykowski A, Nittka M, Wald LL. 32-channel 3 Tesla receive-only phased-array head coil with soccer-ball element geometry. Magn Reson Med 2006;56:216–223. [PubMed: 16767762]
8. Schmitt M, Potthast A, Sosnovik DE, et al. A 128-channel receive-only cardiac coil for highly accelerated cardiac MRI at 3 Tesla. Magn Reson Med 2008;59:1431–1439. [PubMed: 18506789]
9. Sodickson D, Zhang B, Duan Q, et al. Is a “one size fits all” many-element bore-lining remote body array feasible for routing imaging? In Proceedings of the 22nd Annual Meeting of the ISMRM, Milan, Italy, 2014 p. 0618.
10. Nordmeyer-Massner JA, De Zanche N, Pruessmann KP. Mechanically adjustable coil array for wrist MRI. Magn Reson Med 2009;61:429–438. [PubMed: 19161134]
11. Nordmeyer-Massner JA, De Zanche N, Pruessmann KP. Stretchable coil arrays: application to knee imaging under varying flexion angles. Magn Reson Med 2012;67:872–879. [PubMed: 22213018]
12. Corea JR, Flynn AM, Lechene B, et al. Screen-printed flexible MRI receive coils. Nat Commun 2016;7:10839. [PubMed: 26961073]
13. Yan X, Gore JC, Grissom WA. Self-decoupled radiofrequency coils for magnetic resonance imaging. Nat Commun 2018;9:3481. [PubMed: 30154408]
14. Yan X, Gore JC, Grissom WA. A split 8-channel 7T knee coil. In Proceedings of the 26th Annual Meeting of the ISMRM, Paris, France, 2018 p. 4272.
15. Duensing R, Fitzsimmons J, Sanford D, Vazquez J. A continuously variable field of view surface coil. Magn Reson Med 1990;13:378–384. [PubMed: 2325538]
16. Adriany G, Van de Moortele PF, Ritter J, et al. A geometrically adjustable 16-channel transmit/receive transmission line array for improved RF efficiency and parallel imaging performance at 7 Tesla. Magn Reson Med 2008;59:590–597. [PubMed: 18219635]
17. Brown R, Lakshmanan K, Madelin G, et al. A flexible nested sodium and proton coil array with wideband matching for knee cartilage MRI at 3T. Magn Reson Med 2016;76:1325–1334. [PubMed: 26502310]
18. Dornberger B, Vester M, Rehner R, Zenge M, Lattanzi R, Wiggins G. An investigation of coupling and loading effects for adaptive coil design. In Proceedings of the 24th Annual Meeting of the ISMRM, Singapore, 2016 p. 3521.
19. Findeklee C Array noise matching-generalization, proof and analogy to power matching. IEEE Trans Antennas Propag 2011;59:452–459.
20. Wiggins G, Brown R, Zhang B, et al. SNR degradation in receive arrays due to preamplifier noise coupling and a method for mitigation. In Proceedings of the 20th Annual Meeting of ISMRM, Melbourne, Victoria, Australia, 2012 p. 2689.
21. Tilley AR. The Measure of Man and Woman New York, NY: The Whitney Library of Design; 1993.

22. Duan Q, Duyn JH, Gudino N, et al. Characterization of a dielectric phantom for high-field magnetic resonance imaging applications. Med Phys 2014;41:102303. [PubMed: 25281973]
23. Gabriel S, Lau RW, Gabriel C. The dielectric properties of biological tissues: II. Measurements in the frequency range 10 Hz to 20 GHz. Phys Med Biol 1996;41:19.
24. Finnerty M, Herczak J, Zheng T, Weaver J, Yang X, Fujita H. A 3D parallel imaging capable transmit and 15-channel receive array knee coil at 3T. In Proceedings of the 16th Annual Meeting of ISMRM, Toronto, Canada, 2008 p. 1077.
25. Siemens Healthineers, Body 18, https://www.healthcare.siemens.com/magnetic-resonance-imaging/options-and-upgrades/coils/body-18.
26. Siemens Healthineers, CP Body Array Flex Coil and Extender, https://www.healthcare.siemens.com/magnetic-resonance-imaging/options-and-upgrades/coils/cp-body-array-flex-coil-and-extender.
27. Kellman P, McVeigh ER. Image reconstruction in SNR units: a general method for SNR measurement. Magn Reson Med 2005;54:1439–1447. [PubMed: 16261576]
28. Zhang B, Cloos MA, Chen G, Wiggins GC. A size-adaptable electric dipole array for 7T body imaging. In Proceedings of the 24th Annual Meeting of the ISMRM, Singapore, 2016 p. 3508.
29. Vasanawala SS, Stormont R, Lindsay S, et al. Development and clinical implementation of very light weight and highly flexible AIR technology arrays. In Proceedings of the 25th Annual Meeting & Exhibition of the ISMRM, Honolulu, HI, USA, 2017 p. 755.
30. Zhang B, Sodickson DK, Cloos MA. A high-impedance detector-array glove for magnetic resonance imaging of the hand. Nat Biomed Eng 2018;2:570–577. [PubMed: 30854251]
31. Port A, Reber J, Vogt C, et al. Towards wearable MR detection: a stretchable wrist array with on-body digitization. In Proceedings of the 26th Annual Meeting of the ISMRM, Paris, France, 2018 p. 017.

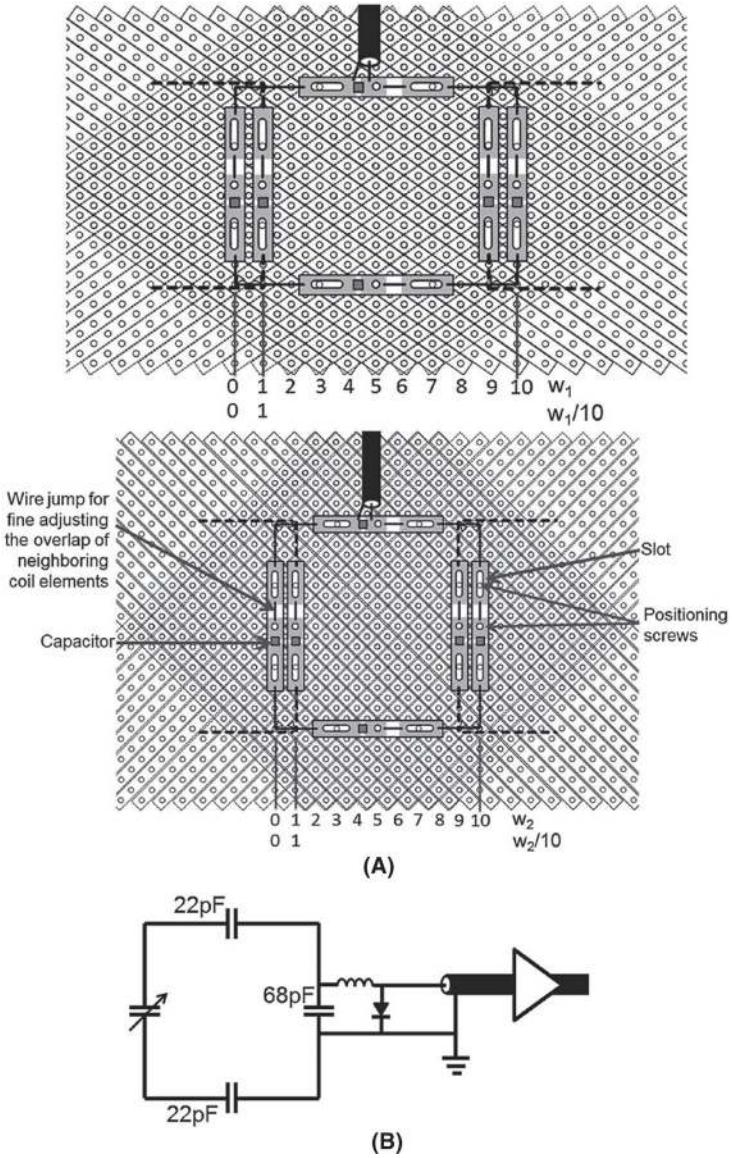

FIGURE 1.

A, Trellis structure used as the holder for the 8-ch array, the use of 10 nylon strips per coil element width allows maintaining a constant 10% overlap between neighbor coils to assure inductive decoupling when the coil size changes. In fact, when the width of each coil element is w_1, the overlap is $0.1 \times w_1$, and when the width of the coil element is squeezed to w_2, the overlap becomes $0.1 \times w_2$. B, Schematic drawing of each coil element in the 8-ch array

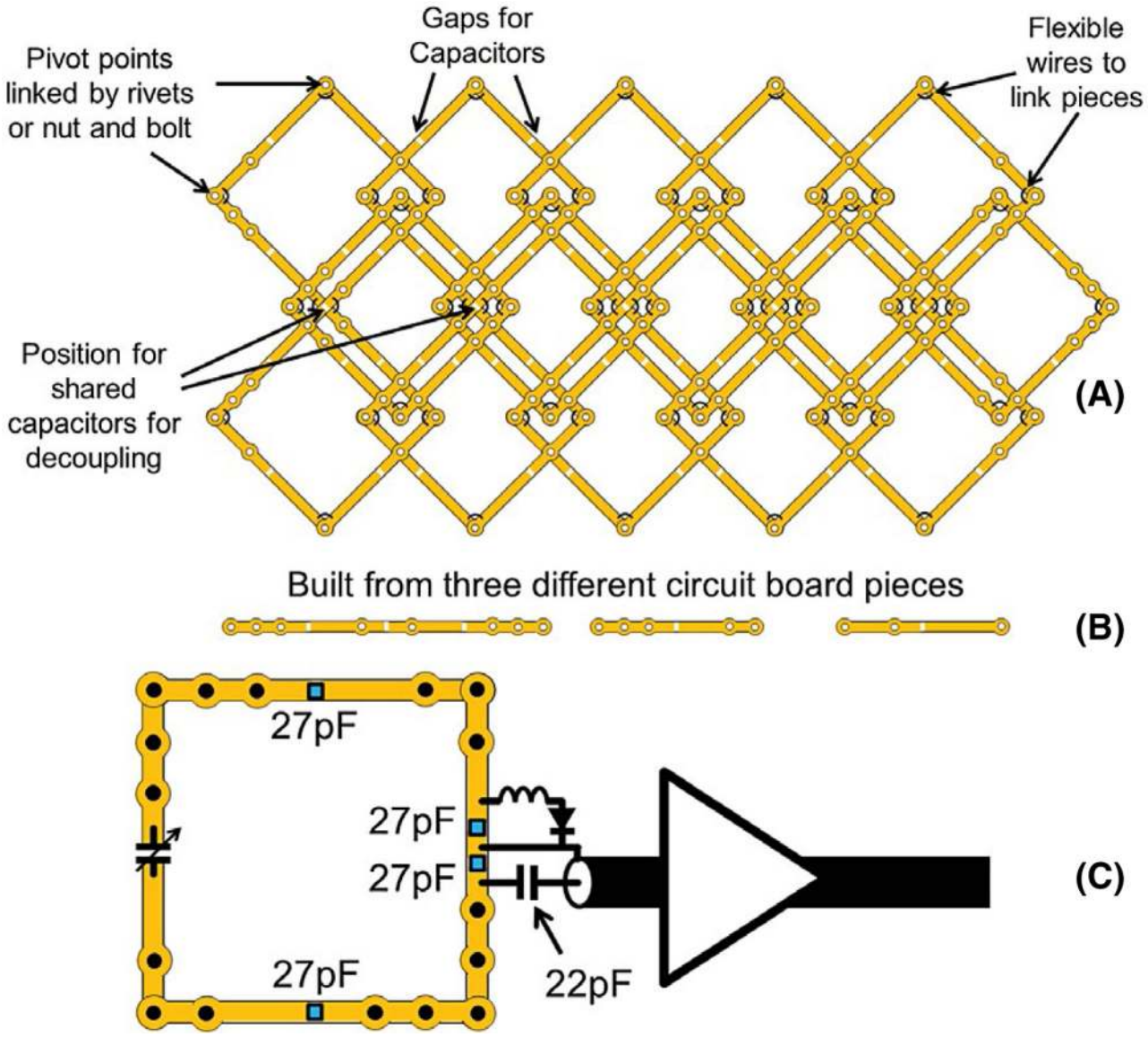

FIGURE 2.

A, Layout of the 24-ch trellis knee coil. The PCBs (yellow) are linked at pivot points by rivets (white circles), whose positions were selected to optimize geometric overlap between neighbor elements for decoupling. The PCBs include gaps (white stripes) for tuning and matching capacitors. Flexible wires (black arcs) were used to link the PCB pieces such that electrical connections were maintained during trellis flexion. B, The 3 basic PCB pieces used to create the array. C, Schematic drawing of each trellis coil element

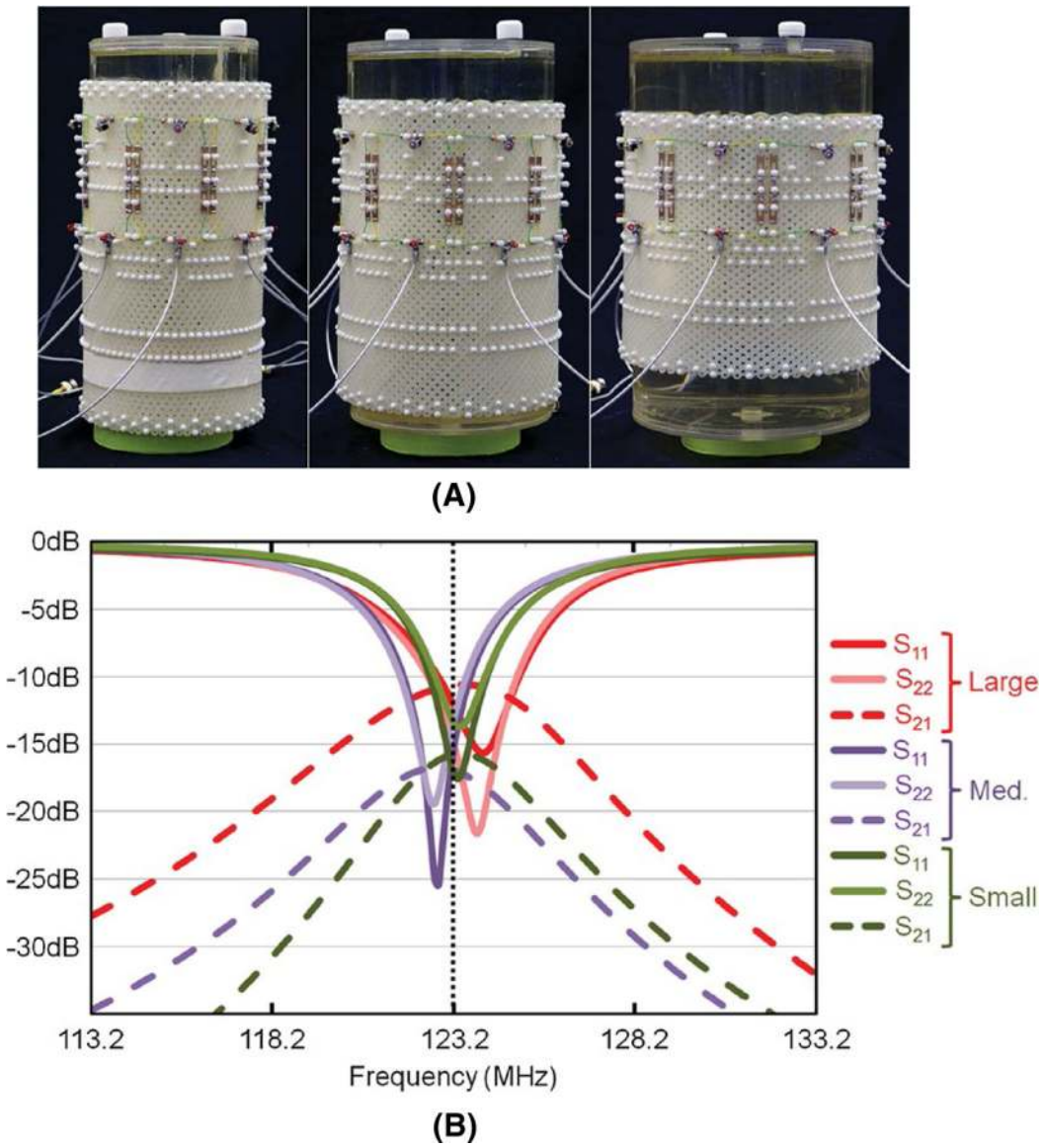

FIGURE 3.

A, photographs of the 8-channel trellis array adapted for 3 phantoms with diameters equal to 134, 165, and 195 mm. B, Parameters of a pair of coil elements in the 8-channel array on 134, 165, and 195 mm phantoms

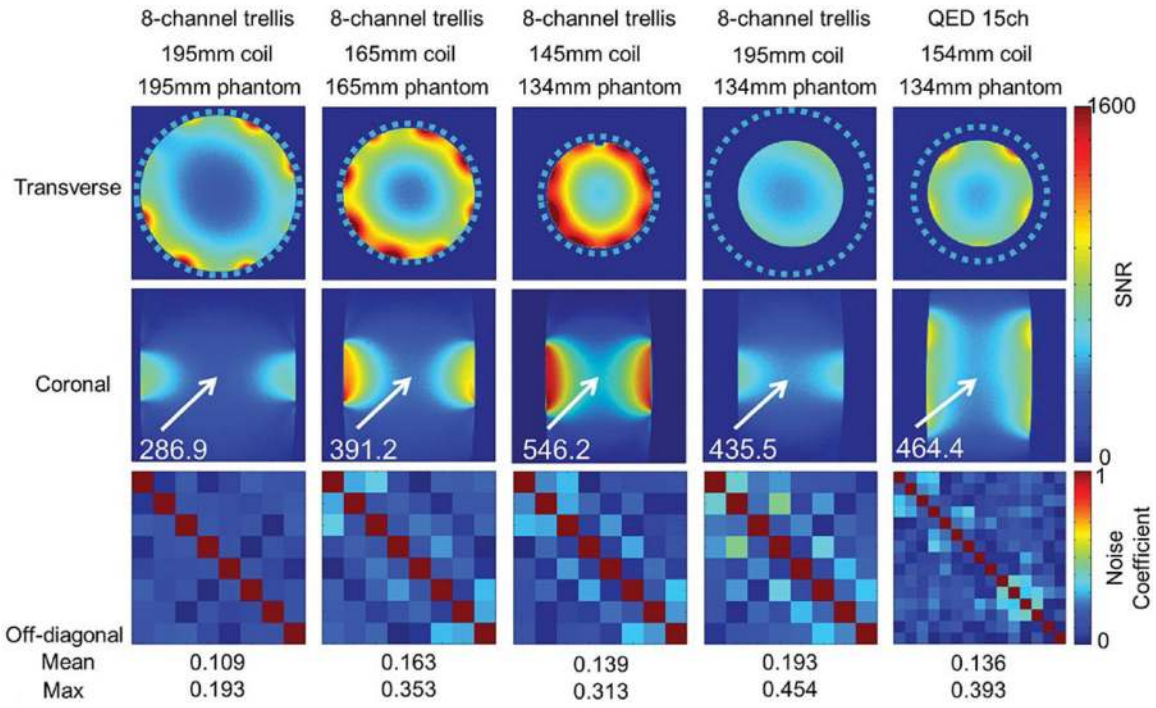

FIGURE 4.

The SNR of the 8-channel trellis array wrapped tightly around phantoms of different size (first 3 columns) and surrounding the smallest phantom, but with the diameter expanded to fit the largest phantom (fourth column), is compared with the SNR of the commercial 15-ch knee array surrounding the smallest phantom (fifth column). Images in SNR units are shown for a central slice in the transversal plane (first row) and coronal plane (second row). The noise coefficient matrixes for each case are shown in the third row

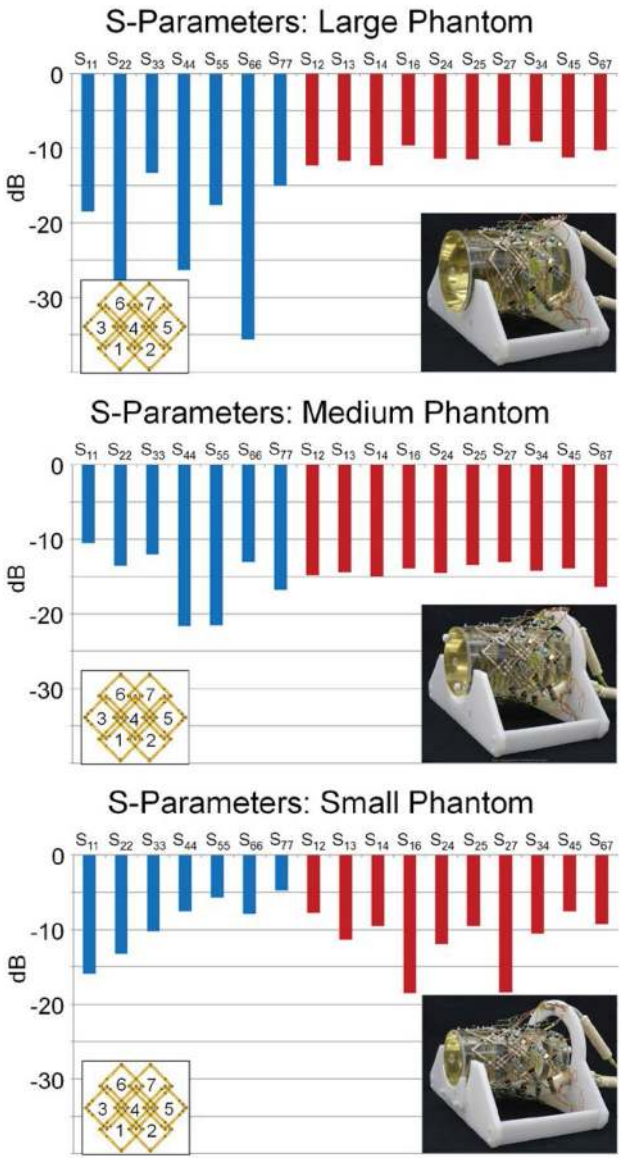

FIGURE 5.
S parameters of a 7-element cluster within the 24-ch trellis array

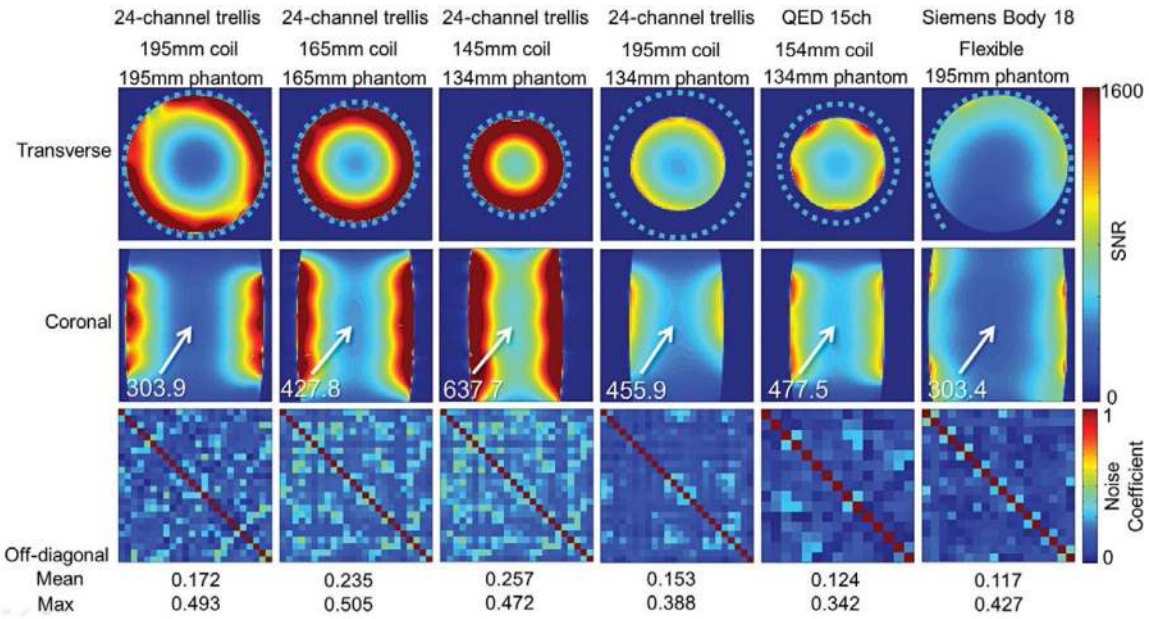

FIGURE 6.

SNR of the 24-channel trellis array adapted to the diameter of different phantoms (first~third columns) and expanded to largest phantom, but used on the smallest phantom (fourth column) is compared to the SNR of the QED 15-channel knee coil for the smallest phantom (fifth column) and Siemens 18-channel flexible body array for the largest phantom (sixth column)

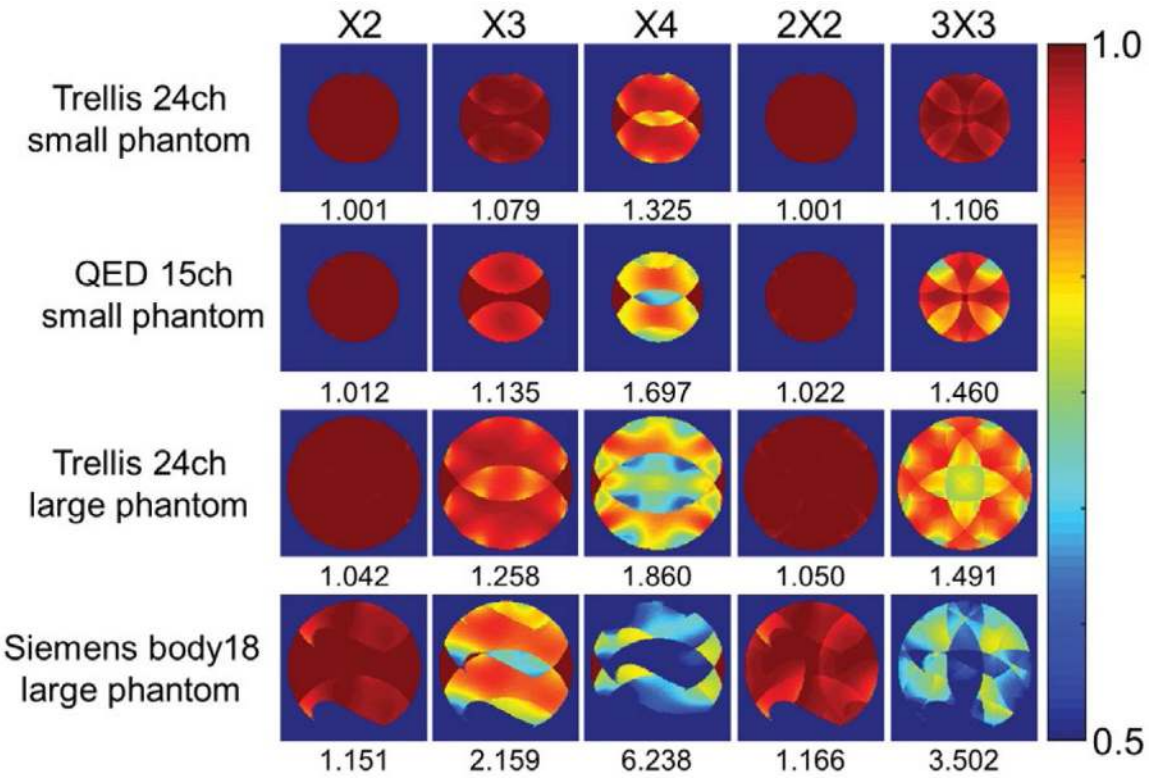

FIGURE 7.

Inverse g-factor (1/g) maps at various 1D and 2D accelerations are shown for the 24-channel trellis arrays for the smallest (first row) and largest (third row) phantom. For comparison, the corresponding maps for the QED 15-channel knee coil and the Siemens 18-channel body coil are shown in the second and fourth row, respectively. Maximum g-factor values within the phantom are reported at the bottom of each map

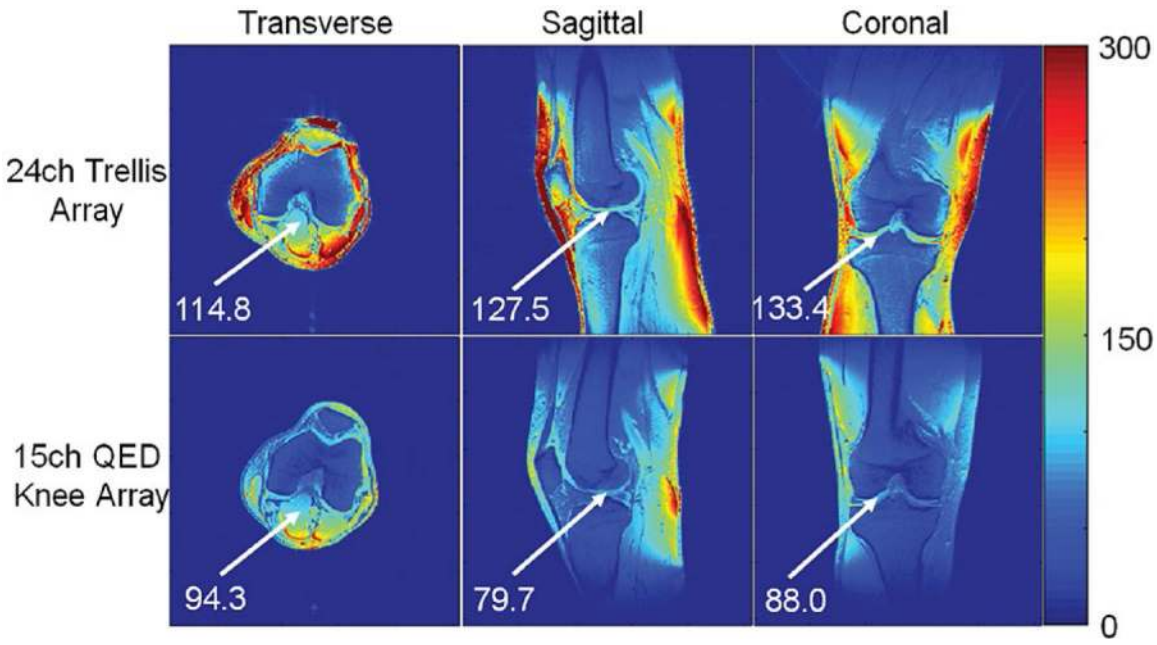

FIGURE 8.

In vivo images in SNR units for 3 orthogonal slices in the knee for the trellis 24-channel array (top row) and the QED 15-channel array (bottom row)

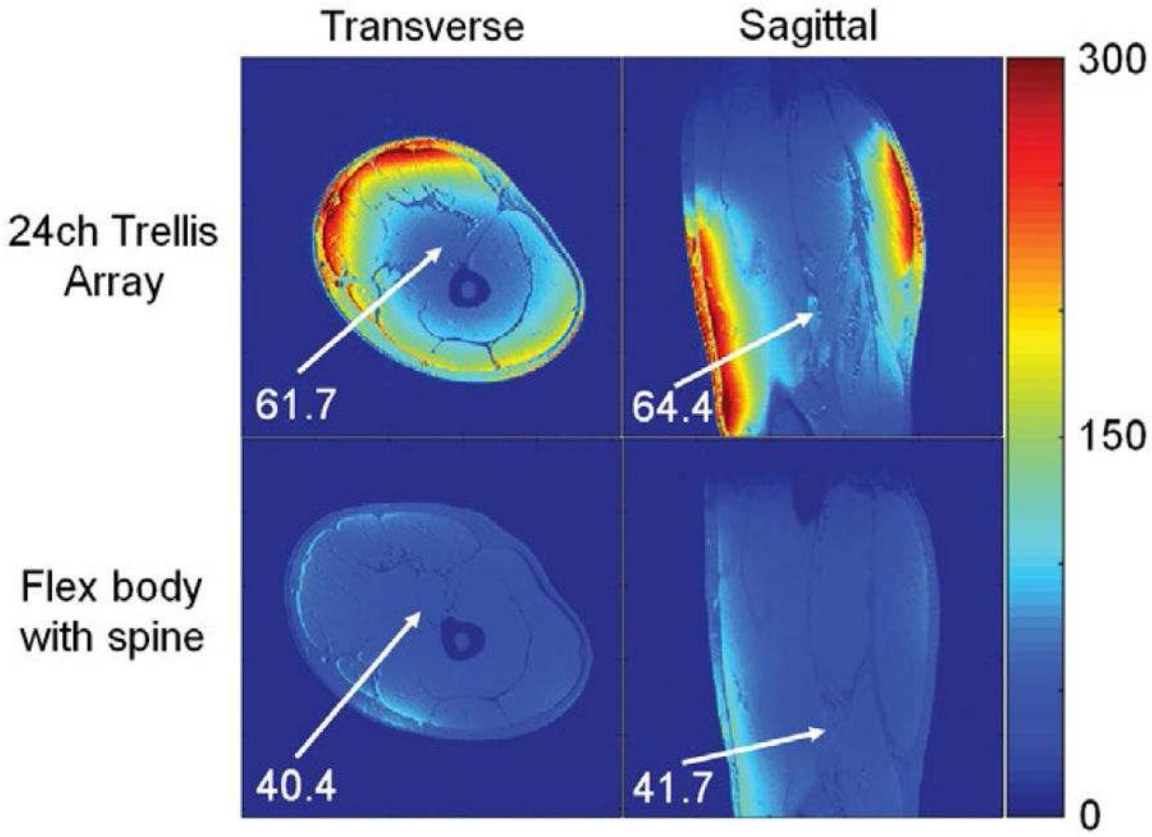

FIGURE 9.

In vivo images in SNR units for 2 orthogonal slices in the thigh (same subject as in Figure 8) for the trellis 24-channel array (top row) and the combination of the system-flexible body with spine array (bottom row)

TABLE 1

Sequence parameters for SNR measurement

	Matrix size	TE (ms)	TR (ms)	Flip angle	Bandwidth (Hz/pixel)	FOV (mm^2)
Phantom imaging	128 × 128	3.92	300	20	300	200 × 200
Knee imaging	256 × 256	3.18	300	20	260	142 × 162
Thigh imaging	256 × 256	3.18	300	20	260	171 × 197

Abbreviation: FOV = field of view.